



# Passively Coded Synthetic Aperture Interferometric Radiometer (CSAIR): Theory and Measurement Results

Ettien Lazare Kpré, Cyril Decroze

## ► To cite this version:

Ettien Lazare Kpré, Cyril Decroze. Passively Coded Synthetic Aperture Interferometric Radiometer (CSAIR): Theory and Measurement Results. European Conference on Antennas and Propagation, Mar 2017, Paris, France. hal-01499414

HAL Id: hal-01499414

<https://unilim.hal.science/hal-01499414>

Submitted on 31 Mar 2017

**HAL** is a multi-disciplinary open access archive for the deposit and dissemination of scientific research documents, whether they are published or not. The documents may come from teaching and research institutions in France or abroad, or from public or private research centers.

L'archive ouverte pluridisciplinaire **HAL**, est destinée au dépôt et à la diffusion de documents scientifiques de niveau recherche, publiés ou non, émanant des établissements d'enseignement et de recherche français ou étrangers, des laboratoires publics ou privés.

# Passively Coded Synthetic Aperture Interferometric Radiometer (CSAIR): Theory and Measurement Results

Ettien Lazare Kpré, Cyril DECROZE  
XLIM research institute, University of Limoges,  
123 avenue Albert Thomas, 87060 LIMOGES CEDEX, France  
E-mail: ettien.kpre@etu.unilim.fr

**Abstract**—Based on the synthetic interferometric imaging technique (SAIR), a new microwave radiometer architecture is proposed in this paper to detect thermal noise sources with a passive coded measurement approach so called CSAIR. In this new system, a passive microwave device is used to intrinsically code and multiplex the antenna signals. This allows the reduction of the number of RF chains while keeping the same antenna array configuration needed in a conventional interferometric radiometers. The system principle is described and the signal processing required for the target brightness temperature rendering is also discussed. Simulation and measurement results show the effectiveness and the potential of the proposed system.

**Index Terms**—Synthetic aperture, radiometry, Microwave imaging, microwave device.

## I. INTRODUCTION

Microwave radiometer are powerful sensors for high-resolution imaging. Nevertheless, due to the trade off between the spatial resolution and the antennas aperture, real aperture radiometer cannot achieve the desired high spatial resolution. Synthetic aperture radiometer has been suggested as an alternate to real aperture radiometer [1]. Indeed, it can synthesize a large aperture from a few sparsely arranging number of antennas. In this way, high spatial resolution can be achieved without any mechanical or electronically scanning [2]. The basic idea is to measure all the possible cross-correlation between each pair of electromagnetic waveforms received by the antennas. These correlation samples are usually called visibility function and their relative positions in the spatial frequency domain are called baselines. In the ideal case, the visibility function is related to the target brightness temperature through a spatial Fourier transform [3]. Numerous radiometers are based on this concept such as the Electronically Scanned Thin Array Radiometer (ESTAR)[4], Microwave Imaging Radiometer using Aperture Synthesis (MIRAS) [5].

Besides the maturity of microwave technologies, high resolution imaging algorithms have greatly improved the conventional interferometric radiometer performances [6]. Thereby, the SAIR technique can be applied to practical near-field applications such as security check, concealed weapons detection, since they require real time acquisition and high spatial resolution. On the over hand, high resolution imaging requires a large number of antennas which is directly linked to the number of RF chains.

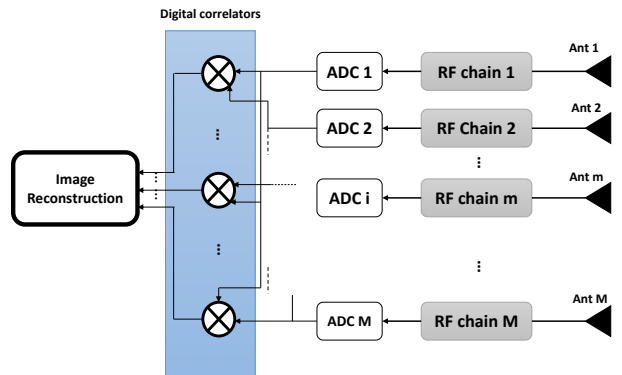


Figure 1. Architecture of a conventional microwave radiometer.

As depicted in Fig.1 a conventional interferometric radiometer architecture consists of an antenna array, where each antenna is connected to a single RF chain, insuring the down-conversion of the RF signal to a digital baseband IQ signal. Then, the ensuing process consists to perform the correlations in pair and image reconstruction. As consequence, the hardware complexity increases as well as the dimensional requirements of the antenna array.

The main contribution of this paper is to propose a new approach using a  $M \times N$  ( $M \gg N \geq 1$ ) ports microwave device whose transfer functions are uncorrelated to intrinsically code the receive waveforms from the  $M$  antennas. Herein, the device frequency diversity is associated to a spatial diversity through  $N$  output ports connected to  $N$  shared RF chains. A generalized visibility function recovering method is introduced and the image reconstruction ensuing. The simulation and experimental results indicate that the new architecture can be an alternate to drastically reduce the complexity of the conventional microwave radiometers while keeping the same antenna array geometry.

## II. CSAIR FUNDAMENTALS

In this section a new radiometer architecture is introduced to reduce the number of RF chains needed in a conventional SAIR architecture. The aim of this concept is to measure the visibility function sample from a compressed acquisition performed in the physical layer. A generic setup of the passive coded SAIR (CSAIR) is described in Fig.2. The receiving antenna array is connected to a  $M \times N$  (Output/Input) ports microwave device

which intrinsically codes and multiplexes the received  $M$  antenna signals into  $N \ll M$  output signals, leading to the architecture simplification. Then the measured signal  $c_n(f)$  ( $n \in [1, 2, \dots, N]$ ) without noise at the device single output in frequency domain can be expressed by:

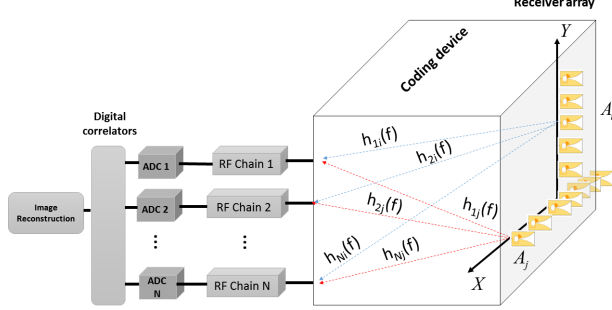


Figure 2. Passive coded SAIR architecture.  $M$  received signals are coded into  $N$  measured signals.

$$c_n(f) = \sum_{m=1}^M h_{nm}(f) s_m(f) \quad (1)$$

where  $h_{nm}(f)$  corresponds to the device transfer function between the antenna  $m$  and the device output  $n$ .  $s_m(f)$  is the received signal by the  $m^{\text{th}}$  antenna. For the sake of efficient description of the principle, Eq.1 can be reformulated for each frequency sample as linear equation bellow:

$$\mathbf{c} = \mathbf{H}\mathbf{s} \quad (2)$$

Where  $\mathbf{c}$  and  $\mathbf{s}$  are respectively  $N \times 1$  and  $M \times 1$  vectors and  $\mathbf{H}$  is  $N \times M$  matrix. Since the principle of the SAIR is to measure the cross-correlation between each pair of the received signals, the challenge is to estimate the individual antenna signal from the aggregate signal  $c_n(f)$ . Therefore, due to the reduction of the number of RF chains, the dimension of the measured signal  $\mathbf{c}$  is significantly less than the received signals  $\mathbf{s}$ . So the Eq.2 is underdetermined equation. Under this ill-posed problem, the most efficient method is the equalization to solve it. A standard approach is to estimate the received signal  $\mathbf{s}_r$  that minimizes the  $l_2$  norm of the objective function defined by [7]:

$$\min \|\mathbf{H}\mathbf{s} - \mathbf{c}\|_2^2 + \mu \|\mathbf{s}\|_2^2 \quad (3)$$

where  $\mu$  is the regularization parameter which can be tuned to obtain a trade-off between the regularization term and the penalty function. The choice for  $\mu$  must be done before inversion. Tikhonov solution is an example of suitable equalization method which can explicitly be formulated as follow:

$$\mathbf{H}_\mu^+ = (\mathbf{H}^\dagger \mathbf{H} + \mu \mathbf{I})^{-1} \mathbf{H}^\dagger. \quad (4)$$

$(.)^+$  and  $(.)^\dagger$  are respectively the equalized pseudo-inverse and the transposed conjugate operators. The received signal can be computed by :

$$\mathbf{s}_{r\mu} = \mathbf{H}_\mu^+ \mathbf{c} \quad (5)$$

The estimated signal can be derived from Eq.2 and Eq.5 by the following relation:

$$\begin{aligned} \mathbf{s}_{r\mu} &= \mathbf{H}_\mu^+ \mathbf{c} \\ &= \mathbf{H}_\mu^+ \mathbf{H} \mathbf{s} \\ &= \mathbf{R}_\mu \mathbf{s} \end{aligned} \quad (6)$$

$\mathbf{R}_\mu$  denotes the pseudo-correlation matrix of the device transfer functions. Ideally this matrix tends to an identity matrix leading to a perfect estimation of the received signal. But this is hardly achievable in practice, limited by the frequency and spatial diversity of the component. Thereby it can be approximated by the use of an oversized metallic microwave cavity which transfer function are uncorrelated [9].

The visibility function between two antennas labeled  $i$  and  $j$  can be computed by:

$$V_{ij}(u, v) = \langle s_{r\mu i}(f) \cdot s_{r\mu j}^*(f) \rangle \quad (7)$$

Based on interferometry fundamentals and first order Taylor approximation, the near-field visibility function is related to the brightness temperature through the following equation[6]:

$$\begin{aligned} V_{ij}(u, v) &= e^{-i\Phi(u, v)} \times \\ &\sum_{\xi^2 + \eta^2 \leq 1} T_M(\xi, \eta) \tilde{r}_{ij} \left( -\frac{u\xi + v\eta}{f_0} \right) e^{i2\pi(u\xi + v\eta)} d\xi d\eta \end{aligned} \quad (8)$$

where  $T_M(\xi, \eta)$  is the modified brightness temperature given by:

$$T_M(\xi, \eta) = \frac{T(\xi, \eta) F_i(\xi, \eta) F_j^*(\xi, \eta)}{\sqrt{1 - \xi^2 - \eta^2}} \quad (9)$$

$(u, v)$  is the relative antennas spacing normalized by the wavelength namely baselines,  $(\xi, \eta)$  are the spatial coordinates of the radiating source,  $T(\xi, \eta)$  is the brightness temperature,  $F_i(\xi, \eta)$  and  $F_j(\xi, \eta)$  are the normalized antennas radiation pattern,  $1/\sqrt{1 - \xi^2 - \eta^2}$  is the oblique factor.  $\tilde{r}(\tau) = r(\tau) e^{-j2\pi f_0 \tau}$  is the so-called fringe wash-function which account for spatial decorrelation effect and depends on the component transfer function through Eq.11 [10]:

$$r_{ij}(\tau) = \int_0^\infty \mathbf{R}_{\mu i}(f) \mathbf{R}_{\mu j}^*(f) e^{j2\pi f \tau} df \quad (10)$$

For an ideal radiometer, this parameter can be neglected whereas for a real CSAIR system, the fringe-wash function can rapidly be significant, thus it is important to take it in account for image reconstruction.  $\Phi(u, v) = \pi(d_i^2 - d_j^2)/\lambda R$  is the quadratic modified term which should be considered for a near-field imaging [6].  $R$  and  $d_i$  are respectively the imaging distance and the antenna euclidean distance from the center of the array. Formulating visibility function and brightness temperature images as vectors of respectively length  $P$  and  $Q$ , Eq.8 can be rewritten in a matrix form [8]:

$$\mathbf{V} = \mathbf{G} \cdot \mathbf{T} \quad (11)$$

Where  $\mathbf{G}$  is the  $P \times Q$ -length system matrix,  $P$  is the number of visibility samples including redundant elements,  $Q$  is the number of reconstructed pixels and  $G(p, q)$  is the  $p^{th}$  row and  $q^{th}$  column component of  $\mathbf{G}$ .

$$G(p, q) = F_i(\xi_q, \eta_q)F_j^*(\xi_q, \eta_q)\tilde{r}_{ij}\left(-\frac{u_p\xi_q + v_p\eta_q}{f_0}\right) \\ \times e^{i(2\pi(u_p\xi_q + v_p\eta_q) - \phi(u_p, v_p))} \quad (12)$$

Finally, a conventional G matrix inversion can be applied to reconstruct the target image [11]. Counter to a simple spatial Fourier transform, the G matrix inversion helps to correct errors due to the fringe-wash function, oblique factor, and antenna patterns. This method is the basis of the image reconstruction in the following sections.

The proposed method is validated by the means of numerical simulations and experiments measurement in the following sections.

### III. COMPUTATIONAL RESULTS AND ANALYSIS

In this section, two numerical scenarios are held to compare the proposed CSAIR concept and the conventional SAIR. The scenarios consist of 16 isotropic antennas arranged along a "T" shaped array as depicted in Fig.3. The antennas are separated by an inter-elements spacing of  $d_x = 0.7 \times \lambda$ , where  $\lambda$  is the central wavelength in the microwave S-Band (2 – 4GHz). The noise sources are assumed to be able to radiate centimeter-wave with a power proportional to their brightness temperature  $T(\xi, \eta)$ . The integration time used for these scenarios is  $\tau = 1\mu s$  with an average factor of 128.

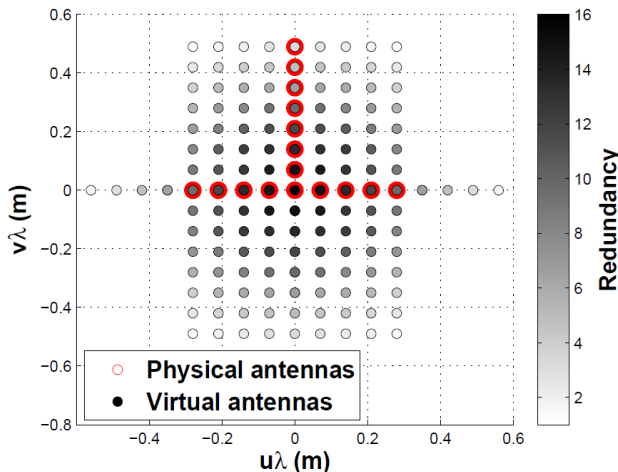


Figure 3. T-shaped antenna array and the corresponding  $(u, v)$  coverage.

In the first scenario, each antenna is directly connected to a single receiver channel as shown in Fig.1. The visibility function is directly calculated by performing the correlation in pair between the received waveforms, while in the second scenario, the antennas are connected to  $16 \times N$  (i.e  $N = 2$ ) microwave device as depicted in Fig.2. A simple analytic model of the component transfer functions is numerically implemented to model an oversized microwave cavity general behavior [12]:

$$h_{nm}(f) = \mathcal{F}[g_{nm}(t)e^{-t/\tau_c}] \quad (13)$$

with  $g_{nm}(t)$  a random Gaussian distribution which is a convenient approximation of the oversized microwave cavity.  $\tau_c$  represents the decay time parameter which is linked to the component quality factor. The decay time is set to  $1\mu s$  in this example. The antenna signals are estimated by the equalization method described in the previous section, the visibility function is thus calculated from Eq.7. Finally, the same imaging algorithm based on Tikhonov regularization [11] is applied to both scenarios for the brightness temperature reconstruction (Eq.11).

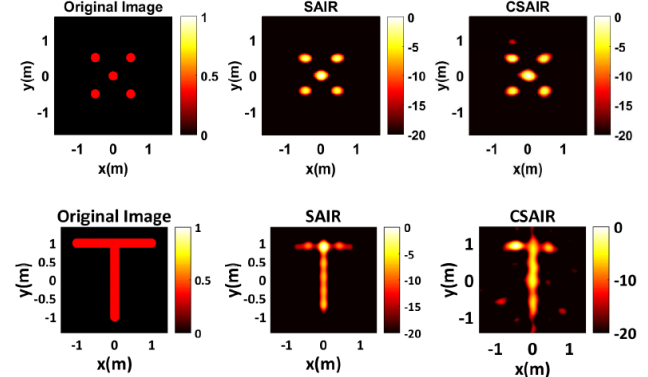


Figure 4. Simulation results of point-like sources and a 'T' shaped 2-D source imaging with conventional SAIR and CSAIR imaging system.

Original point-like sources image is reconstructed considering the two scenarios, especially the conventional SAIR, and the CSAIR as shown in Fig.4. The imaging resolution is about  $(18cm, 28cm)$  for both techniques and the image dynamic is about  $14dB$  for the conventional SAIR and  $10dB$  for the CSAIR. Fig.5 bellow shows the cut-plane along X-axis of the point-like sources image.

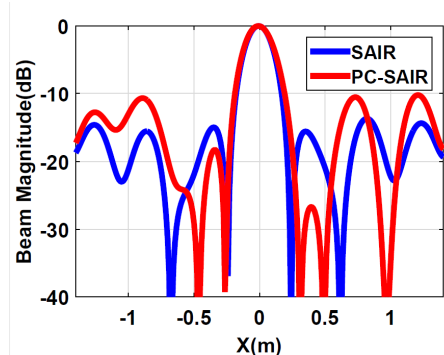


Figure 5. Cut-plane along X-axis of the point-like sources image.

The simulation model was then extended to a 2-D 'T' shaped objects (i.e Fig.4). Even if the dynamic of the CSAIR imaging result is degraded, the image rendering is sufficient to clearly recognize the shape of the object. This demonstrate the effectiveness of the proposed system. Nevertheless, one way to improve the image quality could be to increase the average factor or the spatial diversity (Number of the device output ports).

### IV. MEASUREMENT RESULTS

A measurement platform has been setup to validate the CSAIR concept and the deconvolution strategy. The setup is the same as that introduced in simulation part with 16 Vivaldi antennas designed to match 2 – 4GHz band. The

antennas are arranged in 'T' shape (9 along X-axis and 7 along Y-axis) with an inter-elements spacing of  $dx = dy = 7\text{cm}$ .

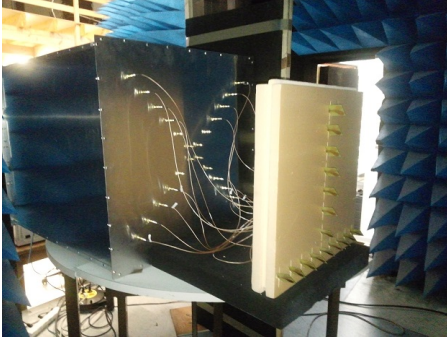


Figure 6. 'T' shaped antenna array connected to the metallic microwave cavity.

Three noise sources are emulated using three 12Gs/s Arbitrary Waveform Generators (Agilent M8190A) connected to three horn antennas. A  $16 \times 2$  ports air-filled metallic cavity with outer dimensions of  $0.8 \times 0.8 \times 1\text{m}^3$  has been utilized as coding device as depicted in Fig.6. The channel transfer functions is pre-characterized and then used as the coding matrix as defined in Eq.1. The noise time integration is  $\tau = 170\mu\text{s}$ . The experience is validated with the 16 Vivaldi antennas connected to the cavity and only two signals are measured by a DSO90404A 20 GSa/s Agilent oscilloscope.

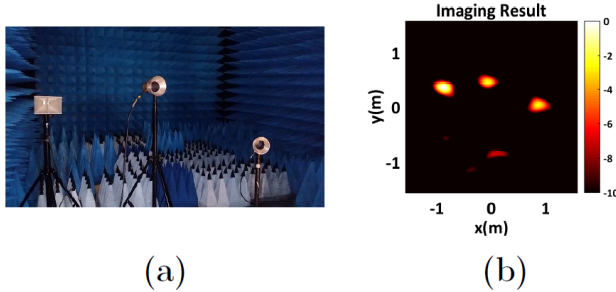


Figure 7. Imaging Results. (a) Three horn antennas used in the noise source emulator. (b) Imaging result of the noise sources.

Fig.7 shows the imaging result of three horn antennas. As it can be noticed, the proposed system is able to detect and discriminate the three sources with only two measured waveforms. The resolution is the same as the theoretical one ( $18\text{cm}$ ,  $28\text{cm}$ ). The imaging result show that the CSAIR can be an efficient alternative of a conventional SAIR since it is cost-efficient technique. Note that in this experimentation, noise signal acquisition has been performed in one shot without any average. This implies that the image dynamic could be significantly improved by implementing averaging on this experimental bench.

## V. CONCLUSION

In this paper, a new synthetic aperture architecture has been proposed based on a passive coding technique performed in the physical layer. Actually a patent is pending on this new approach. In this concept, a microwave coding device is used to intrinsically code and multiplex the  $M$  antenna signals into  $N$  measured waveforms

( $M \gg N \geq 1$ ). Equalization based on Tikhonov method in frequency domain has been applied to estimate the antenna signal needed to reconstruct the target image. The simulation and measurement results show the potential of the proposed system. Since it can drastically reduce the number of RF chains while keeping the same number of antennas, this new approach can obviously be an alternate of the conventional SAIR systems. Future works will focused on an enhanced reconstruction methods and accurate imaging algorithms to reach the conventional SAIR performances. In addition, an important metric to evaluate the performances of the proposed system is the sensitivity  $\Delta T$  which represents the minimum change in temperature of the source that can be detected by the radiometer. Thereby, extended analysis to quantitatively evaluate the sensitivity of the proposed system will be implemented.

## ACKNOWLEDGMENT

This work is supported by the French National Research Agency (ANR) within the framework of the funded project "PIXEL". The authors would like to thank all partners of this project.

## REFERENCES

- [1] C. S. Ruf, C. T. Swift, A. B. Tanner, and D. M. Le Vine, *Interferometric synthetic aperture microwave radiometry for the remote sensing of the Earth*, Geoscience and Remote Sensing, IEEE Transactions on, vol. 26, no. 5, pp. 597–611, 1988.
- [2] J. Dong and Q. Li, *Antenna Array Design in Aperture Synthesis Radiometers*, INTECH Open Access Publisher, 2010.
- [3] F. Zernike, *The concept of degree of coherence and its application to optical problems*, Physica, vol. 5, no. 8, pp. 785 – 795, 1938.
- [4] D. M. Le Vine, *Synthetic aperture radiometer systems*, Microwave Theory and Techniques, IEEE Transactions on, vol. 47, no. 12, pp. 2228–2236, 1999.
- [5] M. Martin-Neira, Y. Menard, J. M. Goutoule, and U. Kraft, *MIRAS, a two-dimensional aperture synthesis radiometer*, in Geoscience and Remote Sensing Symposium, 1994. IGARSS'94. Surface and Atmospheric Remote Sensing: Technologies, Data Analysis and Interpretation., International, 1994, vol. 3, pp. 1323–1325.
- [6] J. Chen, Y. Li, J. Wang, Y. Li, and Y. Zhang, *An accurate imaging algorithm for millimeter wave synthetic aperture imaging radiometer in near-field*, Progress In Electromagnetics Research, vol. 141, pp. 517–535, 2013.
- [7] M. Bertero, P. Boccacci, *Introduction to Inverse Problems in Imaging*, Institute of physics publishing, 1st edition 1998.
- [8] Y. Zhang, Y. Li, S. Zhu, and Y. Li, *A Robust Reweighted L1-Minimization Imaging Algorithm for Passive Millimeter Wave SAIR in Near Field*, Sensors, vol. 15, no. 10, pp. 24945–24960, Sep. 2015.
- [9] T. Fromenteze, E. L. Kpre, D. Carsenat, C. Decroze, and T. Sakamoto, *Single-Shot Compressive Multiple-Inputs Multiple-Outputs Radar Imaging Using a Two-Port Passive Device*, IEEE Access, vol. 4, pp. 1050–1060, 2016.
- [10] M. A. Fischman, A. W. England, and C. S. Ruf, *How digital correlation affects the fringe washing function in L-band aperture synthesis radiometry*, IEEE transactions on geoscience and remote sensing, vol. 40, no. 3, pp. 671–679, 2002.
- [11] E. Anterrieu, *Regularization of an inverse problem in remote sensing imaging by aperture synthesis*, in Acoustics, Speech and Signal Processing, 2006. ICASSP 2006 Proceedings. 2006 IEEE International Conference on, 2006, vol. 2, pp. II–II.
- [12] David A. Hill *Electromagnetic Theory of Reverberation Chambers*, Radio-Frequency Technology Division Electronics and Electrical Engineering Laboratory National Institute of Standards and Technology 325 Broadway Boulder, Colorado 80303-3328.
- [13] N. A. Salmon, J. Beale, J. Parkinson, S. Hayward, P. Hall, R. Macpherson, R. Lewis, and A. Harvey, *Digital beam-forming for passive millimetre wave security imaging*, in Antennas and Propagation, 2007. EuCAP 2007. The Second European Conference on, 2007, pp. 1–11.